CM²

MAGAZINE

第 18 期

创刊词

海洋是生命的摇篮，是文明的纽带。地球上最早的生命诞生于海洋，海洋里的生命最终进化成了人类，人类的文化融合又通过海洋得以实现。人因海而兴。

人类对海洋的探索从未停止。从远古时代美丽的神话传说，到麦哲伦的全球航行，再到现代对大洋的科学钻探计划，海洋逐渐从人类敬畏崇拜幻想的精神寄托演变成可以开发利用与科学研究的客观存在。其中，上个世纪与太空探索同步发展的大洋科学钻探计划将人类对海洋的认知推向了崭新的纬度：深海（deep sea）与深时（deep time）。大洋钻探计划让人类知道，奔流不息的大海之下，埋藏的却是亿万年的地球历史。它们记录了地球板块的运动，从而使板块构造学说得到证实；它们记录了地球环境的演变，从而让古海洋学方兴未艾。

在探索海洋的悠久历史中，从大航海时代的导航，到大洋钻探计划中不可或缺的磁性地层学，磁学发挥了不可替代的作用。这不是偶然，因为从微观到宏观，磁性是最基本的物理属性之一，可以说，万物皆有磁性。基于课题组的学科背景和对海洋的理解，我们对海洋的探索以磁学为主要手段，海洋磁学中心因此而生。

海洋磁学中心，简称 CM^2，一为其全名"Centre for Marine Magnetism"的缩写，另者恰与爱因斯坦著名的质能方程 $E = MC^2$ 对称，借以表达我们对科学巨匠的敬仰和对科学的不懈追求。

然而科学从来不是单打独斗的产物。我们以磁学为研究海洋的主攻利器，但绝不仅限于磁学。凡与磁学相关的领域均是我们关注的重点。为了跟踪反映国内外地球科学特别是与磁学有关的地球科学领域的最新研究进展，海洋磁学中心特地主办 CM^2 Magazine，以期与各位地球科学工作者相互交流学习、合作共进！

"海洋孕育了生命，联通了世界，促进了发展"。 21 世纪是海洋科学的时代，由陆向海，让我们携手迈进中国海洋科学的黄金时代

目 录

谈自己对科研的认识

王敦繁

"自己对科研是否感兴趣，是否对科学充满兴趣，还是这只是一种生活和事业的选择？"很多时候会我会经常这样问自己，但经常也没有准确的答案。最后发现自己其实对什么是科学家，什么是做学问搞研究，这些基本的东西也没有一个准确的理解，所以要理解科研，对其有个准确的认识，实在是空中楼阁，雾里看花。所以，要谈对科研的理解，首先得谈谈自己对科学家和做研究的认识。

你对一个事物的看法和认识，很多时候是基于你与之有关的那些经历所决定的。在自己的研究生教育经历中，一开始的感觉科研就是发文章，看文献，开组会，甚至都没认识到更多的应该是做实验。记得硕士一年级的时候，对科研的认识还是一件很云里雾里的事情,因为当时课题组老师主要是做石油勘探研究的,所以大多都接一些油田项目。这些项目偏生产，与甲方接触的频率要比在实验室呆的频率多很多，许多事情是如何为甲方做好他们需要的服务，所以甲方的需求往往要比研究出什么东西来的更重要，再者，真要研究些什么，那也是师兄师姐的事情，低年级基本就是打打杂，给师兄师姐好好干活，最后同一个方向里博士带几个硕士，硕士拣点东西毕业就行，不会一个人去做一个方向，这样就没有自己去探索，去挖掘的学习过程，所以在这种情况下自己对科研的理解就是简单的发文章，按师兄师姐吩咐做事就行。现在想来真的是不要太肤浅，随后，因为自己感觉得做点海洋的东西，一折腾和老师商量去了深海所联合培养，之后的经历让自己对科研和做研究的理解有了进一步新的认识。记得当时一开始老师把我叫过去聊了聊，结束时给了我一个概念让我下去学一学，然后除了定期问问我进展怎么样就没有下文了，自己脑海中期待的那种跟着老师在实验室学仪器操作，听老师讲实验步骤设计的原理，以及老师教你该如何从文献中寻找突破点的美丽而又梦幻的场景全都像泡沫一样虚幻无影，根本不存在。存在的只是自己看着摸不着脑门的实验步骤和完全没法看的实验结果，但是在产出端老师盯着你呀，隔那么几周你得拿点东西出来讨论讨论，所以在实验室不管明不明白，看着文献简单

设计一下实验流程就摸着石头过河上手做了，慢慢的自己意识到开始的那些痛苦到后面渐渐的好像换回了些什么，自己开始懂一些东西，然后回想起文献里说的，这时候会恍然大悟原来文献里说的就是这么回事！这段经历对自己最大的影响就是懂了一个道理：事情得自己做，有时候别人不会手把手教你，就算手把手教了，那也和你自己经历一段迷茫和阵痛后搞清楚的收获是不一样的，对同一件事情的理解和认识程度也是不一样的。所以，真正学会走路的孩子都是自己摔过跟头的，这时候也理解了老师为什么这样做，其实他就像教孩子学游泳一样，主要做的就是在岸上看着你别溺水就行。硕士期间的经历让自己懂得了科研一开始可能都是从迷茫中出发，摸索前行，螺旋式上升的一个过程，所以这里面一开始坚持住往下做就很重要，在过程中寻找突破要比站在原点规划更有效率，只有坚持慢慢推进，才能慢慢积累进度和收获结果。其实，这条经验不仅在做实验时适用，同样的道理，在生活中很多事情也往往如此需要我们在迷雾中寻找方向，学会在过程中坚持和寻找突破。硕士毕业，自己脑海中的科研，就是如此。这个过程中最重要的收获就是学会了怎么去做事情，尽管不知道这个方法是不是完全的正确，但至少明白了当你做一些自己不懂而又需要做的事情的时候就应该这样，出发在路上最重要。

然而，当时的自己可能只懂了点怎么做事情，但还没懂为什么要做这件事情。比如我知道应该这样做，但在做之前却不知道为什么去做，结果和意义是什么。所以感觉博士一开始的状态就是不懂我就先做，做着做着就懂了，至于后面会有什么结果不去深究。这是自己博士第一学期常犯的错误，所以每次也会被老师问："你这样做是为什么，假设就算你做出来了会有什么用呢？解决了什么问题呢？"面对这样的问题自己常常是一脸茫然。最后自己脑海中反思了好几回，觉得做事情之前得清楚目的，看一件事得清楚它的目的，过程，结果以及意义，做科研尤其得如此，这样才能形成系统。要以问题为导向，不然工作做了很久，最后回过头来可能发现只是做了点东西，不会有什么成体系突破性的收获。另外一点比较重要的是，在做科研的过程中不能看到别人做什么出成果了自己也去蹭热度做。向外寻求突破要比与人抢夺更长远更可持续，世界是离散均匀的，任何一个方向做足做细同样会有好的成果出现。博士半年，自己对科研的认识就是如此。有人说一个人成长的过程就是：头撞到墙（困难）——摸头反思（思考）—

—伸出头往前（实践）——再头撞到墙。。。的无限循环之中，在困难、思考、实践的过程中一厘米一厘米往前螺旋式上升。虽然这个小循环自己经历了，但可能在科研这架螺旋梯上，自己还只处在最低那一层。海拔在头顶，还需在迷茫与阵痛中坚持向前行。

第 8 章　磁化率概念进四阶

磁化率和温度、频率有关系，这非常好理解。磁化率和外加场还有关系吗？

这又可以分为两种情况。当外加场很小的时候，无论是单畴还是多畴，它的磁矩变化可逆，所以大部分仪器都用低场（比如 0.4 mT＝4 Oe）磁化样品，进行磁化率测量。MPMS 系统一般设置为 0.4 mT 这个量级。外场再大，磁矩变化可能就变为不可逆。

除了这个原因，我们要对尼尔理论进行一点扩展：

$$\tau = \tau_0 \exp\left(\mu_0 V M_S H_K / kT^* (1-H_0/H_K)^2\right)$$

和之前的公式相比较，我们会发现在分母那里多了一个小后缀（$1-H_0/H_K$）。微观矫顽力 H_K 是 mT 级别，外加磁场 H_0 则是 μT 级别，差了好几个数量级。可见，随着 H_0 逐渐增大，沿着 H_0 的方向，τ 会逐渐减小。而在外场的反方向，τ 会随着外场增大逐渐增大。也就是说，颗粒更加容易平行于 H_0 的方向排列。

外场能够影响 SD 颗粒的 τ，而 τ 又和 T_B 正相关，因此，外场的改变也能引起 SD 颗粒的解阻温度的改变。具体来讲，随着外场的增大，其解阻温度向低温方向移动。

对某些大的 SD 颗粒，其解阻温度高于 300 K，也就是说需要加热才能让其解阻。可是，加热会影响物质化学稳定性，这可怎么办呢？

我们不妨把外场加大一些，当然，肯定不能加到很大，要适当！比如尝试把外场从 4 Oe 加大到 8 Oe。这时候，样品的 T_B 可能就会降低到 300 K 之下，不用往高温加热，也可以探测到样品的解阻行为了。

目前，相对于磁化率的频率和温度特性，对其外加场特性研究还不够深入。从原理上讲，驰豫时间 τ 也是外加场和 H_K 的函数，由于不同矿物的 H_K 不同，其磁化率随着 H_0 的变化曲线也不尽相同。因此，可以通过研究 K-H 曲线来区分一些具有不同矫顽力的矿物行为。MFK 磁化率仪器已经拥有了 K-H 测量方式。

对于铁磁性和亚铁磁性物质（比如单质铁、磁铁矿和磁赤铁矿），其磁化率最高。相较之下，反铁磁性物质（比如赤铁矿和针铁矿）的磁化率则低得多。因

此，样品中即使含有很少量的磁铁矿和磁赤铁矿，样品的磁化率也常常受它们控制。这在中国黄土和古土壤中表现得非常明显。黄土高原的古土壤中含有大量的赤铁矿，从绝对含量上来看，赤铁矿才是主导矿物，但是，古土壤的磁化率却是由磁赤铁矿控制。

对于比较大的 SD 磁铁矿，当样品完全均匀氧化成磁赤铁矿时，由于 Ms 的整体降低，其磁化率会降低。但是对于刚好处于 SP/SD 临界值之上的磁铁矿颗粒，当它均匀氧化成磁赤铁矿时，由于驰豫时间减小，会从 SD 状态变为 SP 状态，反而使磁化率大幅度增加。对于粒径很粗的准单畴（PSD）、多畴颗粒，很难被均匀氧化，一般会在颗粒的表面形成细颗粒的磁赤铁矿膜，这样其整体磁性的变化就会非常复杂。

当磁性矿物的晶格中含有杂质时，其磁化率随着矿物的纯度（Stoichiometry）的降低而呈复杂的变化。比如，对于纯的赤铁矿和针铁矿，其磁性非常低。当晶格中含有微量杂质时（比如铝），其磁性会随着铝含量的变化而变化。

这涉及到两种截然不同的影响。

反铁磁性物质的磁性很低，这是因为相邻两层（A 和 B）Fe^{3+} 的磁矩完全反向，互相抵消。如果掺入一些杂质，并优先替代某一层中的 Fe^{3+}，会使得这两层 Fe^{3+} 的含量不再相等，从而整体上产生磁性。但是，如果 Al^{3+} 在 A 层和 B 层是均匀替代，那么就不会产生额外的磁性。由于 Al^{3+} 没有磁性，反而会产生稀释效应，让磁性整体降低。

有了这个模型基础，我们来看看合成样品的性质。当 Almol%<6%时，含铝赤铁矿（Al-Hm）的磁化率下降，说明 Al^{3+} 在 A 层和 B 层几乎时均匀替代 Fe^{3+}，稀释作用占主导，磁化率下降。之后，Al-Hm 的磁化率随着 Al^{3+} 替代浓度的增加而增加。这说明，Al^{3+} 开始在某一个面优先替代。或者粒径变化发挥作用了，逐渐从 SD 向 SP 转换。

上面的实验没做完，如果 Al^{3+} 的含量继续增加，会出现什么效果？

我们考虑一个极端情况，那就是 Fe^{3+} 全部被 Al^{3+} 替代，形成 Al_2O_3，变成无磁性的。所以我们可以百分百判断，随着 Al^{3+} 含量继续增加，磁化率会先达到一个峰值，然后开始下降。

还有一个问题，如果合成 Al-Hm 的化学环境发生变化，上述的磁性行为是

否也会变？

Al^{3+}替代 Fe^{3+}的模式肯定会受到合成环境的影响。不同的合成路径应该会造成不同的影响。如果谁重新再合成一批 Al-Hm，其磁化先升后降也不是不可以。这就说明在他的合成实验条件下，Al^{3+}从一开始就在某一层优先替代 Fe^{3+}。

赤铁矿被 Al^{3+}替代后，性质变化很大。如果一直抱着纯赤铁矿的眼光来分析地质问题，就会出现潜在的错误解释。

影响磁化率的因素很多，通过详尽的综合性研究，可以精确地解释其变化机制及影响因素，进而确定相关的地质与环境过程。

首先判断样品的磁化率(χ_{bulk})是否小于零。如果是，那么样品的磁性就由抗磁性占主导，比如石英、碳酸钙等。这种情况一般比较少见。但是对于石笋和珊瑚等材料，研究其磁化率就得多加小心。

如果样品的磁化率大于零，下一步要进行幅值判断。通常把样品的磁化率与样品的顺磁磁化率进行归一化(χ_{bulk}/χ_{para})。如果这个值接近于 1，说明样品的磁化率主要受顺磁性矿物控制，铁磁性矿物的含量很少。值得注意的是，χ_{para} 一般由磁滞回线的高场线性部分拟合获得。样品中反铁磁性矿物(比如针铁矿)在高场一般也不会饱和，从而会使得χ_{para} 值偏大。可以通过 CBD 处理前后样品的χ_{para} 来估算反铁磁性矿物对χ_{para}的影响。

如果$\chi_{bulk}/\chi_{para}>1$，说明样品中含有铁磁性矿物。接下来可以通过更详细的实验来确定铁磁性矿物的磁畴状态。如果$\chi_{fd} >0$，且χ与χ_{fd}正相关，说明χ受到纳米颗粒的控制。如果χ与χ_{fd}不相关，说明样品中纳米颗粒的含量不够高，样品的磁化率主要受到大颗粒 PSD/MD 颗粒的控制。

如果$\chi_{fd} =0$ 或者χ_{fd} 很小，可以对应着两种截然不同的情况。首先这可能暗示着样品中不含有 SP 颗粒，而以粒径为大颗粒占主导，这些大颗粒不具有磁化率频率特性。第二种情况是样品中所含的 SP 颗粒粒径很小，在室温也不具有频率特性。低温测量可以进一步区分这两种结果。

如果频率磁化率曲线在低温出现峰值，也就是对应着解阻行为，暗示着确实存在着小粒径的 SP 颗粒，其解阻温度小于室温。值得注意的是，如果χ_{fd}的峰值出现在 50 K，还需要排除 MD 颗粒的干扰。相比较于 SP 颗粒，MD 颗粒更易于被磁铁吸出来。去除 MD 颗粒后，如果样品的 50 K χ_{fd}峰值消失，说明这个χ_{fd}峰

值主要由 MD 颗粒携带。还可以应用 CBD 处理技术来区分 SP 和 MD 颗粒的性质。

磁化率除了本身可以作为磁学参数外，还可以与其它参数配对提供更多的信息。应用最多的是 χ 与 χ_{ARM} 的比值(与之相关的是 King-Plot)。χ/χ_{ARM} 在 SD 粒径区间达到最小值(~0.09)，在向更小或者更大的粒径区间展布时，又会增加。因此，整体上随着粒径的增加，χ/χ_{ARM} 呈"M 字形分布。除此之外，还有 $\chi_{ARM}/SIRM$、$SIRM/\chi$、χ/M_s 等比值参数。其中，χ/M_s 常用来衡量 SP 的贡献。对于大颗粒的磁铁矿，其 $\chi/M_s < 10^{-5}$ m/A，当这个比值比较大时，暗示着样品中存在着大量的 SP 成分。在环境磁学研究中，综合运用这些比值参数，往往能得到有用的磁粒度信息，而磁性颗粒的粒度常常是与地质与环境过程密切相关的。

以上讨论表明，影响磁化率的因素非常多。对于不同的地质和气候环境，磁化率的变化机制也不尽相同。实际工作中首先需要确定磁化率的主要贡献者，最常用的手段是磁化率随着温度变化的高低温曲线，通过各种特征点（包括各种磁性转换点和居里温度点）来判定磁性矿物的类型。需要注意的是，在高温阶段，有可能会生成新的磁性矿物。此时，可以利用逐步加热曲线来确定磁性矿物转化的温度点。这样还可以识别在居里温度前的磁化率峰到底是霍普金森峰还是新生成的磁性矿物引起的。与之配套的还有一些前期处理样品的手段。比如，应用 CBD 方法分离仅由 Fe^{3+} 构成的铁氧化物（主要是磁赤铁矿、赤铁矿、针铁矿）与粗颗粒磁铁矿贡献。此外，还可以通过筛选和重力分异等方法把样品首先分为不同的粒级组分，然后衡量每一组分对整个样品的磁性贡献。

当把磁化率的变化与具体的地质和环境过程相联系时，需要知道背景值的信息。比如，在某一自然沉积物剖面，如果发现磁化率在某一深度向上突然增加，这既可以解释为上覆沉积物中磁性矿物含量增加（比如中国黄土-古土壤序列），又可以解释为下伏沉积物中磁性矿物被溶解（比如，近海岸表层海洋沉积物）。下面通过实例简要探讨如何应用磁化率变化特征来获取陆相和海相沉积物记录的地质、环境过程的信息。

黄土在全球范围内广泛分布，其中最为著名的是中国的黄土-古土壤序列。在冰期时，冬季风搬运来大量粉尘物质，在黄土高原沉积下来，形成黄土层；在间冰期时，粉尘输入减少，同时夏季风带来丰富的降雨，形成土壤层。因此，在

冰期-间冰期旋回的时间尺度上，形成黄土-古土壤的交互序列。前人研究表明，简单的磁化率测量就可以分辨出这种黄土-古土壤韵律。经成土作用，古土壤中形成大量的SP/SD磁赤铁矿，使得古土壤的磁化率显著升高。由于应用了磁化率作为东亚夏季风的替代指标，极大地推动了中国黄土古全球变化的研究。通过黄土-古土壤序列的磁化率和深海氧同位素记录的对比，开辟了海陆气候耦合研究的新途径，使得中国黄土在全球气候变化研究领域占有举足轻重的地位。然而，在世界其它地区（比如西伯利亚、阿拉斯加、阿根廷等），古土壤的磁化率不仅不升高，反而降低。在西伯利亚、阿拉斯加地区，磁化率的变化主要受到冬季风强弱控制。当冬季风较强时，搬运来的碎屑磁性矿物粒径较大，因而磁化率较高。而在阿根廷地区，古土壤的低磁化率特征则是由于暖期的大量降雨导致溶解作用占主导，使得整体磁性减弱。

磁化率在海相沉积物研究中也被广泛应用，是大洋钻探计划(ODP 和 IODP)科考船上的必测参数之一。在北太平洋地区，由于缺少构建氧同位素曲线的物质，Tiedemann and Haug (1995)把磁化率作为冰筏物含量的替代指标，并进一步进行了轨道调谐，从而得出比较合理的时间标尺。在地中海地区，大量的粉尘物质来源于撒哈拉沙漠地区。Larrasoaña et al. (2008)发现在该区磁化率可以作为粉尘物质含量的替代指标。Rohling et al. (2008)则发现红海沉积物中记录的$\delta^{18}O_{ruber}$ (海平面记录)与南极冰盖记录变化一致，而磁化率的变化（内陆粉尘的替代指标）则与北极冰盖记录一致。直接对比两种记录发现了海平面变化与内陆粉尘（局部气候，或者与季风相关）存在着相位差。Brachfeld (2006)成功地应用高场顺磁磁化率来研究海洋沉积物中生物成因物质的含量变化。然而，海相沉积物的磁化率实际也受到多种因素控制，比如，物源磁性矿物的种类和含量、自生磁性矿物的种类和含量、磁性矿物的保存程度，以及生物成因的抗磁性物质的稀释作用（比如碳酸盐）。

除了以上的例子，磁化率还在其它地质环境领域被广泛应用。比如，湖相沉积物的地层对比和古环境重建、油气田上方的油烟囱、海相地质填图、城市污染示踪等。但不同环境或不同的地质过程对磁化率有着十分复杂的影响作用。总之，磁化率并非一个简单的磁学参数，它是多种因素共同作用的综合信息，正确解释磁化率的变化机制必须建立在对相关地质与环境过程的正确理解的基础上。

思考题

1. 对于球形的磁铁矿 $N_a = N_b$，是不是其矫顽力为零？

2. 对于磁铁矿，其 $M_s = 480000\,A/m$，如果 $N_b - N_a = 0.3$，请计算其矫顽力，单位规一化为 mT， $1mT = 780\,A/m$

3. 磁铁矿形状各项异性能占主导，赤铁矿为磁弹性能占主导，一般来说，谁的矫顽力大些？

4. 一般情况下，磁铁矿的矫顽力为几十个 mT，请问磁铁矿的矫顽力能不能超过 100mT？在特殊情况下，磁铁矿的矫顽力最大为多少？

5. 假设实验观测所需时间为 1 秒，颗粒每转换一次状态需要 2 秒，$\tau = 2S$， 我们能否准确地观测到其状态？在什么样的情况下，我们不能观测到颗粒的状态？如果观测不到颗粒的状态，我们称之为什么状态？

6. 在室温为 SP 状态的颗粒，如何才能使其处于 SD 状态？

7. 在室温，一个磁铁矿颗粒刚好处于 SP 与 SD 的转换状态，对于同样大小的磁赤铁矿颗粒，它处于什么状态？

8. 在室温，两个体积相等，但形状不同的磁铁矿颗粒，长条形的磁铁矿颗粒刚好处于 SP 与 SD 的转换状态，那么另外一个立方体的磁铁矿颗粒它处于什么状态？

9. 磁铁矿的居里温度为 578 度，其解组温度为多少？

10. 如果一台仪器的工作温度最大量程是室温，而一块样品中磁性矿物的解阻温度大于室温，应用什么技术可能测量该样品的解阻行为？

文献导读

1. 中全新世时期太平洋深层水扩张进入南大洋

翻译人：仲义 zhongy@sustech.edu.cn

摘要： 南大洋是研究全球大洋环流系统中水团翻转和混合作用的关键区域。因为南大洋动态变化受控于南半球西风带（SWW）控制，西风带的控制作用会很大程度地控制该区域的水团循环和混合作用。虽然全新世以来（11,700 年以来）南半球西风带（SWW）控制变化已经被证实，但是对于其海洋的响应变化还存在争议。本文中利用具有确切年龄的冷水珊瑚骨骼的 Nd 同位素含量来示踪全新世以来南大洋水团变化特征，结果显示，在中全新世极大期（距今 7000-6000 年），以现今水深分布来看主要以上层绕极深层水（UCDW）组成，表现出太平洋水团的 Nd 同位素特征。我们认为，在中全新世时期极向南半球西风带（SWW）作用减弱，导致南大洋深水混合作用降低，进而太平洋深层水加剧进入 UCDW，使得水团结构明显与现今环流特征不同。晚全新世极向的 SWW 作用进一步增强，通过改变表层水层密度差增强水团混合作用，进而促进大量 CO_2 进入到大气当中。

ABSTRACT: The Southern Ocean is a key region for the overturning and mixing of water masses within the global ocean circulation system. Because Southern Ocean dynamics are influenced by the Southern Hemisphere westerly winds (SWW), changes in the westerly wind forcing could significantly affect the circulation and mixing of water masses in this important location. While changes in SWW forcing during the Holocene (i.e., the last ~11,700 y) have been documented, evidence of the oceanic response to these changes is equivocal. Here we use the neodymium (Nd) isotopic composition of absolute-dated cold-water coral skeletons to show that there have been distinct changes in the chemistry of the Southern Ocean water column during the Holocene. Our results reveal a pronounced Middle Holocene excursion (peaking ~7,000–6,000 y before present),

at the depth level presently occupied by Upper Circumpolar Deep Water (UCDW), toward Nd isotope values more typical of Pacific waters. We suggest that poleward-reduced SWW forcing during the Middle Holocene led to both reduced Southern Ocean deep mixing and enhanced influx of Pacific Deep Water into UCDW, inducing a water mass structure that was significantly different from today. Poleward SWW intensification during the Late Holocene could then have reinforced deep mixing along and across density surfaces, thus enhancing the release of accumulated CO_2 to the atmosphere。
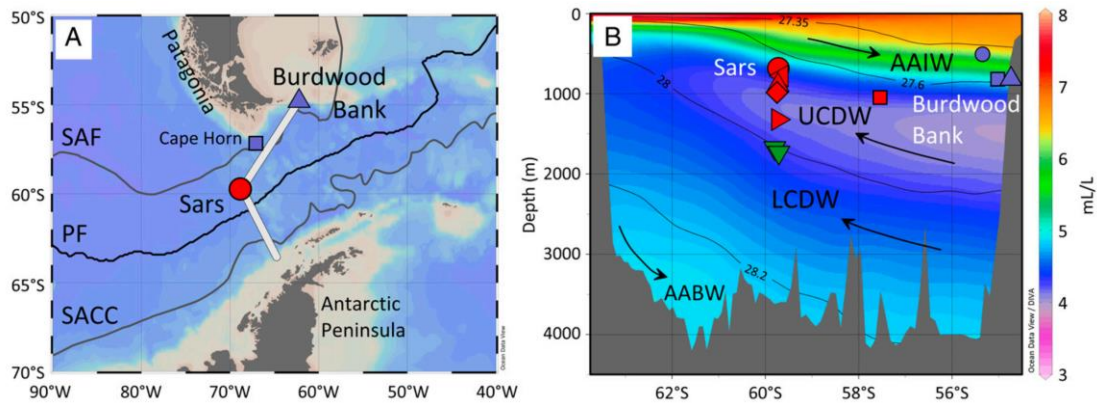

Figure 1. Sample locations of Southern Ocean cold-water corals. (A) Map of Drake Passage coral sampling locations at Sars Seamount (red), Cape Horn, and Burdwood Bank (blue). White line demarks section shown in B. Thin gray and black lines indicate the mean positions of the Subantarctic Front (SAF), the Polar Front (PF), and the Southern ACC front (SACC) (3). (B) Oxygen concentration section across the Drake Passage (4). Pacific Southern Ocean (blue-filled circle and redfilled square) and Cape Horn (blue-filled square) sampling locations were transferred into the Drake Passage section density structure relative to the mean frontal positions. All other symbols indicate Sars Seamount and Burdwood Bank sampling locations (SI Appendix, Table S1). Symbol color coding according to the modern water mass structure in red (UCDW), green (LCDW), and blue (AAIW). Thin black lines indicate surfaces of neutral density anomaly γn (in kg/m³) (5). Black arrows indicate the Southern Ocean overturning circulation, i.e., the direction of upwelling deep waters and downwelling intermediate and bottom waters north and south of the PF, respectively. Note the PDW-derived O_2 minimum at UCDW depths. Base map and oxygen section were generated with ODV software.
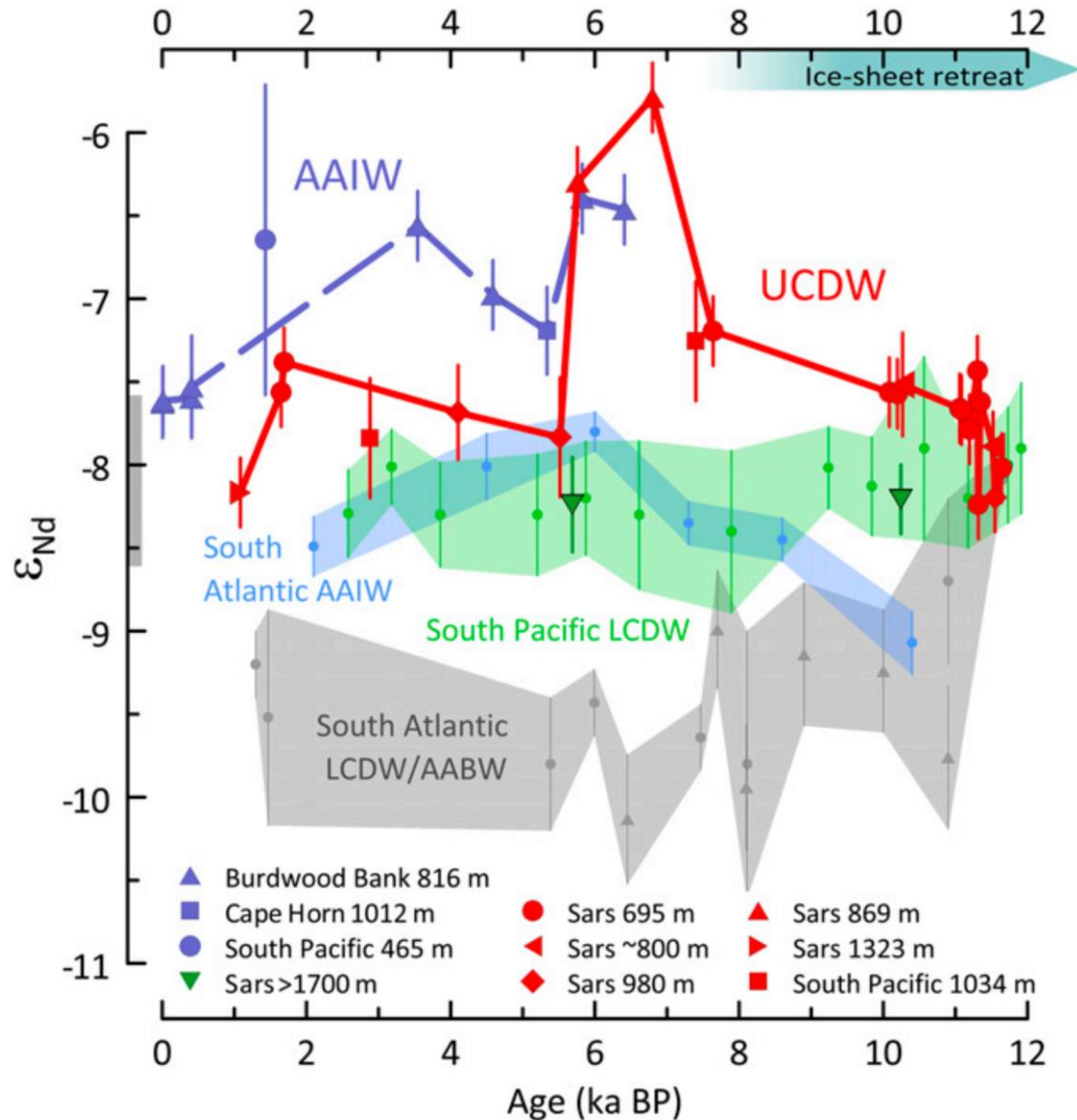
Figure 2. Results from Holocene Southern Ocean cold-water corals. Coldwater coral Nd isotope results from the Drake Passage (including <0.5 ka BP coral data from ref. 24) and the South Pacific. Also shown for comparison are previously published Nd isotope records from South Atlantic LCDW/AABW (gray shading) cores TNO57-21 (4,981-m water depth; site 8) (gray triangles) and MD07-3076 (3770 m water depth; site 7) (gray circles), South Pacific LCDW core PS75/073–2 (3,234-m water depth; site 3) (green shading; not including measurements with analytical uncertainty >1 eNd), and South Atlantic AAIW core GeoB2107-3 (1,048-m water depth; site 6) (lightblue shading). Site numbers refer to locations shown in SI Appendix, Fig. S1. The gray bar at the y axis represents the 2 SD range of Burdwood Bank and Sars Seamount seawater Nd isotopic compositions (γn = 26.93– 28.23 kg/m3, eNd = -8.1 ± 0.5, 2 SD, n = 18; see also SI Appendix, Fig. S3). The green bar indicates the Early Holocene phase of major grounding line retreat of ice sheets in the Pacific sector of Antarctica.
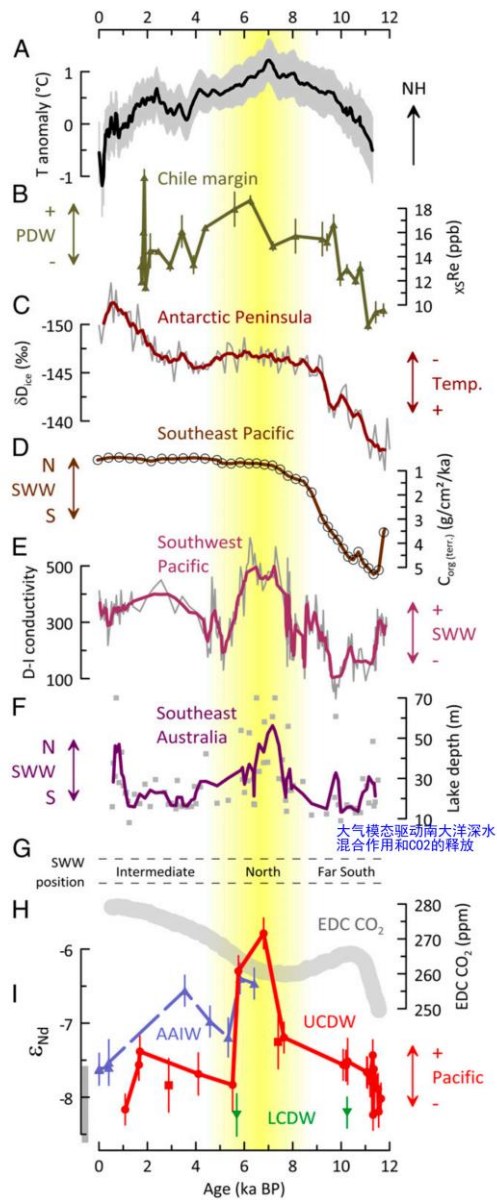
Figure 3. Drake Passage water mass mixing compared to Holocene climate parameters. All site numbers refer to locations shown in SI Appendix, Fig. S1. (A) Interhemispheric extratropical temperature anomaly, where positive values represent Northern Hemisphere positive anomalies and vice versa. (B) Excess rhenium (XSRe) from 1,015-m water depth off Chile, located at hinge depth between high O2 (AAIW) and low O2 (PDW) (site 5). (C) Antarctic Peninsula deuteriumisotope-based temperature record from James Ross Island (note reversed axis) (site 10). (D) Accumulation rate of terrestrial organic carbon in a Patagonian fjord, recording SWW-induced fluvial input (site 4). (E) Diatom-inferred conductivity as a tracer for SWW-controlled sea spray on Macquarie Island north of the PF (site 2). (F) Depth of southeast Australian Lake Gnotuk, indicative of SWWdriven precipitation–evaporation (P-E) balance (site 1). (G) Summary panel of the latitudinal SWW trends, with peak northward intensity between ~7.5 and 5.5 ka BP highlighted by the yellow shading. (H) EPICA Dome C (EDC) ice core CO2 record (11-point running mean) (site 13). (I) Drake Passage Nd isotope data from UCDW (red), LCDW (green), and AAIW depths (blue) (this study and <0.5 ka BP coral data from ref. 5). Gray bar at the y axis represents the range of modern local seawater Nd isotopic compositions (see legend of Fig. 2 for details). Thick colored lines in C, E, and F are 3-point running means of the respective datasets.

13

2. 夏威夷地幔柱中含有一种同位素亏损的下地幔成分

翻译人：冯婉仪 fengwy@sustech.edu.cn

摘要： 大多数洋岛玄武岩都能采集到一种同位素亏损的地幔成分，但这种成分的来源尚不清楚。它可能来自上地幔，也可能来自地幔柱固有的下地幔储库。对于夏威夷而言，同位素亏损的成分主要采集于次生复活阶段的火山活动，该火山活动发生在最初的盾状阶段火山活动之后的 0.5-2 Ma。然而，这种成分也被推测出现在盾状和后盾状熔岩中。我们对一套 Mauna Kea 盾状期拉斑玄武岩的放射性同位素和微量元素组成进行了分析，发现它们与复活期拉斑玄武岩具有相同的同位素组成。我们利用微量元素模型表明这些盾状阶段玄武岩可以解释为由复活阶段地幔源区发生更高程度部分熔融而产生的熔体。因此，我们的数据表明复活阶段的同位素亏损组分是直接采集于盾状阶段的火山活动。盾状阶段和次生复活阶段的火山活动具有共同物质来源，这表明复活阶段的同位素亏损成分是夏威夷地幔柱固有的。进一步推断，夏威夷地幔柱可能起源于下地幔，其所在的地幔区域也是同位素亏损的，这与上地幔相似，但并不完全相同。

ABSTRACT: Most ocean island basalts sample an isotopically depleted mantle component, but the origin of this component is unclear. It may come from either the entrained upper mantle or from a reservoir intrinsic to the plume, sourced from the lower mantle. For Hawaii, the isotopically depleted component is primarily sampled during the secondary rejuvenated-stage volcanism, 0.5-2 million years after the initial shield-stage volcanism. However, it is also inferred in shield and post-shield lavas. We analyse the radiogenic isotopic and trace element compositions of a suite of Mauna Kea shield-stage tholeiites, and found that they have the same isotopic compositions as rejuvenated-stage lavas. We use trace element models to show that these shield-stage basalts can be explained as higher degree partial melts of a rejuvenated-stage source. Our data, therefore, show that the depleted rejuvenated-stage component was directly sampled during shield-stage volcanism. The common source for both shield-stage and secondary rejuvenated volcanism implies that the depleted rejuvenated component is intrinsic to the Hawaiian mantle plume. It is further inferred that the

mantle region from which the Hawaiian plume originates, probably in the lower mantle, is also isotopically depleted, similar but not identical to the upper mantle.
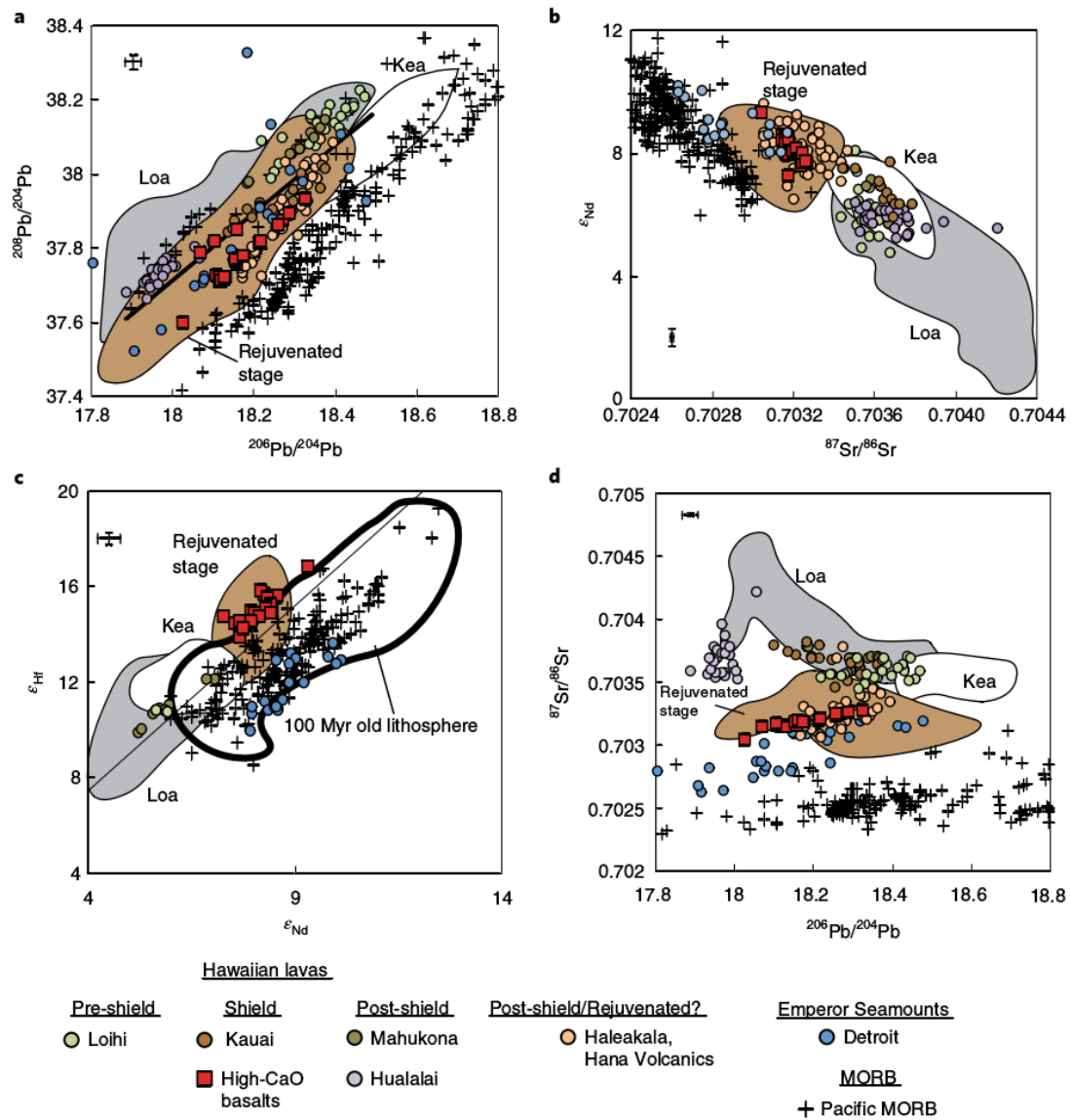

Figure 1 Radiogenic isotope data of Mauna Kea high-CaO basalts relative to shield-stage basalts of both Hawaiian Kea and Loa-trend volcanoes, rejuvenated-stage basalts and Pacific MORBs. a–d, $^{208}Pb/^{204}Pb$ versus $^{206}Pb/^{204}Pb$ (a), εNd versus $^{87}Sr/^{86}Sr$ (b), εHf versus εNd (c) and $^{87}Sr/^{86}Sr$ versus $^{206}Pb/^{204}Pb$ (d). The thick line in a is the dividing line between Kea- and Loa-trend shield basalts58. The diagonal black line in c is the terrestrial array[62] and the field outlined with a thick black line in c is the calculated 100 Myr old lithosphere after MORB generation (Supplementary Information gives details). Error bars represent the two-standard error of measurements. Literature data sources are given in the Supplementary Information.
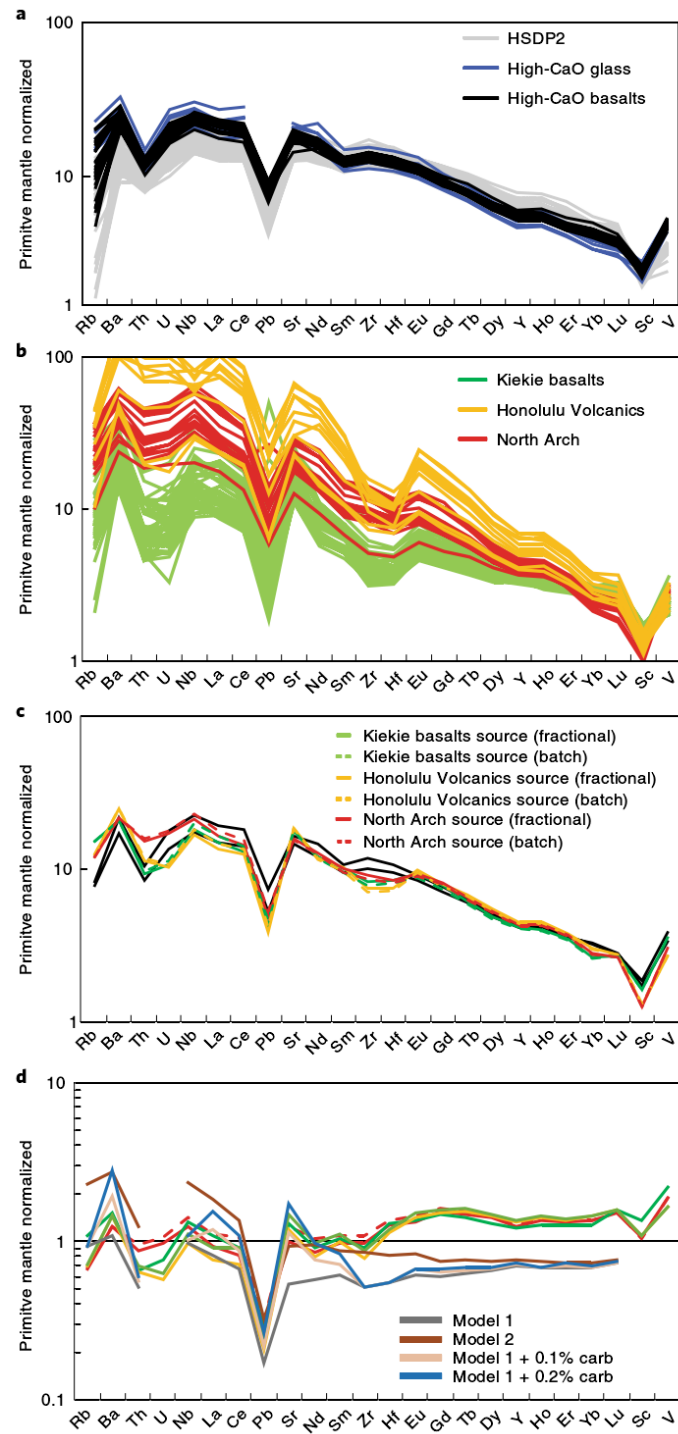
Figure 2. Trace element patterns and models. a, Primitive mantle-normalized trace element patterns for the HSDP reference suite samples (data references are in the Supplementary Information), high-CaO basalts (this study) and high-CaO glasses[42] corrected to Fo_{90} by adding or subtracting olivine. b, Rejuvenated-stage lavas from Honolulu Volcanics on Oahu, North Arch Volcanic Field and Kiekie basalts from Niihau, corrected to Fo_{90} by adding or subtracting olivine, used for the partial melting model. c, Results of our partial melting model relative to the range of values for high-CaO basalts enveloped by the two black lines. d, Calculated source compositions in this study (same key in c) compared to those of Dixon et al.[12] (key in d). 'Carb' in d is carbonatite[12]. The Supplementary Information give details and data sources.

3. 快速的表层流驱动大西洋浮游植物缓慢向北极扩张

翻译人：蒋晓东 jiangxd@sustech.edu.cn

摘要：随着温度升高和海冰回退北极海洋生物系统收缩，该区的生态变化通过北大西洋的连接而与低纬度环境密切相关。大西洋海水携带热量经欧洲北极走廊（作为进出北极 80%水流的通道）向北冰洋流动，同时还携带营养物质和浮游植物。本研究使用卫星监测衍生的高度测量观察技术，发现北大西洋表层流的流速在过去 24 年增长了两倍，而且塑造了颗石藻（Emiliania huxleyi）的空间分布—一种可示踪温和生态系统的藻类。研究结果表明，引起南部物种（例如 Emiliania huxleyi）向北极入侵的主要因素是生物对流，而不是先前认为的水温驱动。本研究也确定，北冰洋中生物和物理上的"大西洋化"很可能改变北极的海洋食物网和生物地球化学循环。

ABSTRACT：The Arctic marine biome, shrinking with increasing temperature and receding sea-ice cover, is tightly connected to lower latitudes through the North Atlantic. By flowing northward through the European Arctic Corridor (the main Arctic gateway where 80% of in- and outflow takes place), the North Atlantic Waters transport most of the ocean heat, but also nutrients and planktonic organisms toward the Arctic Ocean. Using satellite-derived altimetry observations, we reveal an increase, up to two-fold, in North Atlantic current surface velocities over the last 24 years. More importantly, we show evidence that the North Atlantic current and its variability shape the spatial distribution of the coccolithophore Emiliania huxleyi (Ehux), a tracer for temperate ecosystems. We further demonstrate that bio-advection, rather than water temperature as previously assumed, is a major mechanism responsible for the recent poleward intrusions of southern species like Ehux. Our findings confirm the biological and physical "Atlantification" of the Arctic Ocean with potential alterations of the Arctic marine food web and biogeochemical cycles.
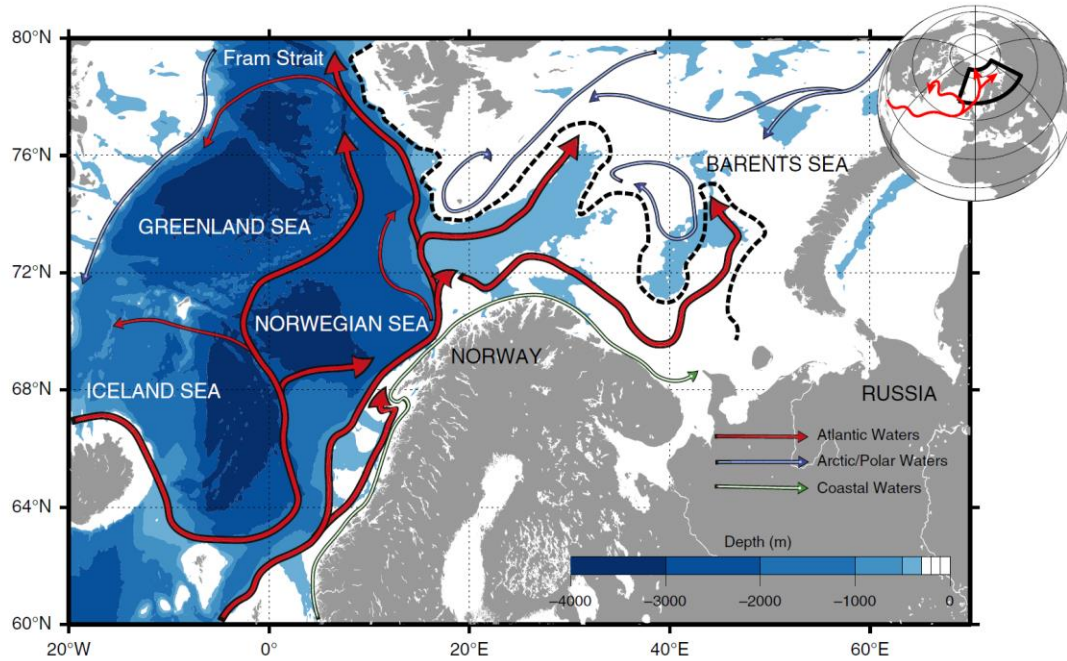
Figure 1. The European Arctic Corridor (EAC). Bathymetry and surface circulation. The Atlantic currents are in red, the Arctic or Polar Waters are in blue and the Coastal Waters are in green. The southern Barents Sea Polar Front is illustrated in black dashed line and separates the Atlantic Waters from the colder and fresher waters from the North.
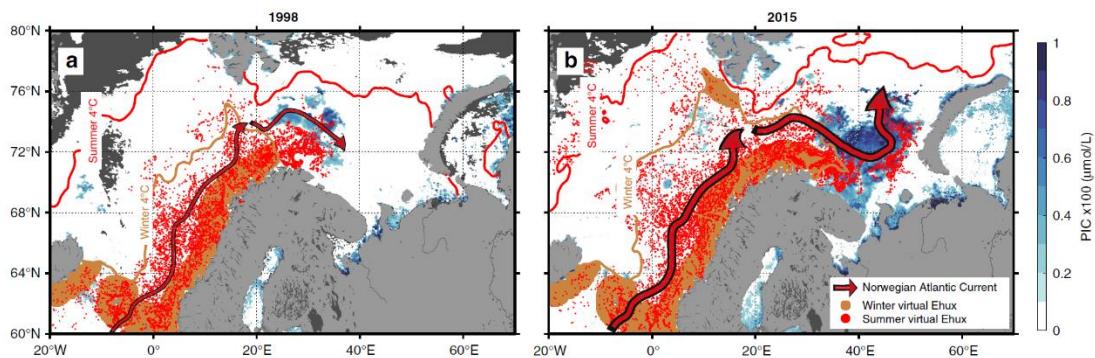

Figure 2. Poleward expansion of Emiliania Huxleyi (EHux) in the European Arctic Corridor. Comparison between 1998 (**a**) and 2015 (**b**). The initialization (inoculum) of virtual particles in March are illustrated by brown dots. During 6 months, particles drift with the Norwegian Atlantic Current (red arrows) as the ocean seasonally warms as illustrated by the northward expansion of the 4 °C isotherm. In August, the particles end up in positions indicated by the red dots. In the background, remotely sensed PIC indicating coccolithophore biomass in summer (July–August–September) is shown in blue colors. Areas with no data are in dark gray.
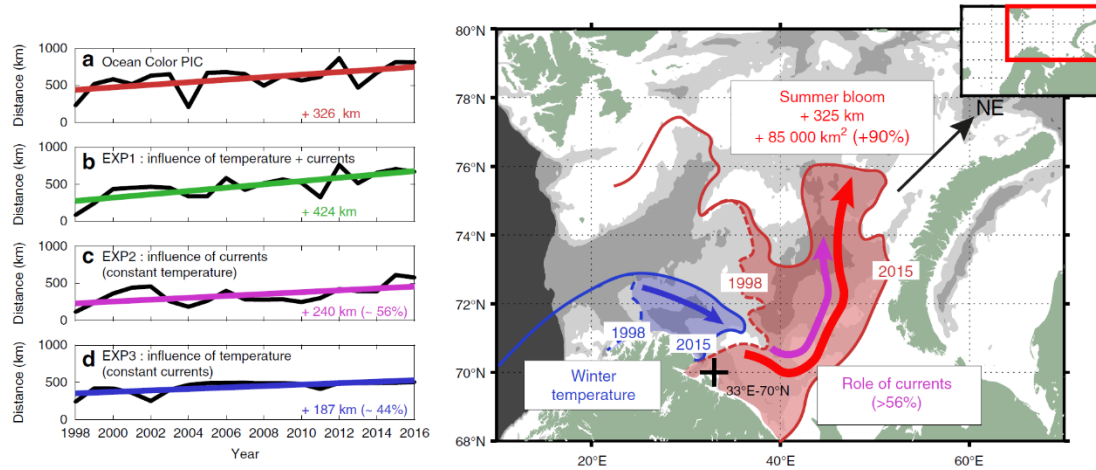
Figure 3. Shifting position of the leading-edge Ehux bloom distribution. Shifting position from ocean-color PIC (**a**), and the 3 Lagrangian experiments (**b**–**d**) for the last 19-years (1998–2016). The comparison between the 1st Lagrangian experiment (EXP1, **b**) with the 2nd (EXP2, **c**) and the 3rd (EXP3, **d**) aims at estimating the relative contribution of currents (EXP2, constant temperature) vs. temperature (EXP3, constant currents) on the total Ehux poleward expansion (EXP1, varying temperature and currents). The right panel is a schematic illustration of the poleward expansion of the Ehux with the winter 4 °C isotherm (lowest temperature for a 'regular' Ehux growth) in blue and the summer bloom position (northern boundary) in red. The two extreme years 1998 (dashed) and 2015 (solid) are represented. Arrows indicate the contribution from temperature and/or currents keeping the same color code.

4. 地球行星磁场

翻译人：柳加波 liujiabo7@gmail.com

摘要：地球磁场是迄今为止已知行星中记录最为详细的磁场。通过融合各种不同记录方法，以及地表岩石悄然记录地磁场的大部分历史，我们对地球磁场特性和性质的理解已取得了可观的进步。地球磁场在导航方面的作用，以及个别人的奉献精神，促成了科学史上最长的定量观测记录之一。最近，人们从太空中获得了更加系统的地磁观测结果，从而能够比以前更详细地研究地球磁场。计算机能力的逐步提高也至关重要，这引起了处理和分析大量地磁观测数据方法的改进。计算机的可行性，再加上数值模拟的最新发展，使得研究地球磁场成为地球科学领域中一个非常活跃的领域。在本文，我们尝试概述科学界目前对地球磁场的研究进展，包括观测、解释和理解由地核引起的主磁场在过去和现在的变化。我们将介绍不同类型的地磁数据并解释它们各自的特征。之后，如果具有可行性，我们将描述如何利用这些数据建立随时间演化的地磁场信息，否则，我们将只描述这些数据的统计信息。需要特别注意是，解释如何将不同的数据整合在一起得出信息，以及如何进一步一致地描述地磁场在过去的变化。最后，我们回顾了从年到上亿年尺度上对地磁场变化的解释，强调了磁流体动力学在地核中的作用和整个行星的缓慢动态演化所起到的作用。

ABSTRACT： The magnetic field of the Earth is by far the best documented magnetic field of all known planets. Considerable progress has been made in our understanding of its characteristics and properties, thanks to the convergence of many different approaches and to the remarkable fact that surface rocks have quietly recorded much of its history. The usefulness of magnetic field charts for navigation and the dedication of a few individuals have also led to the patient construction of some of the longest series of quantitative observations in the history of science. More recently even more systematic observations have been made possible from space, leading to the possibility of observing the Earth's magnetic field in much more details than was previously possible. The progressive increase in computer power was also crucial, leading to advanced ways of handling and analyzing this considerable corpus of data. This possibility, together with the recent development of numerical

simulations, has led to the development of a very active field in Earth science. In this paper, we make an attempt to provide an overview of where the scientific community currently stands in terms of observing, interpreting and understanding the past and present behavior of the so-called main magnetic field produced within the Earth's core. The various types of data are introduced and their specific properties explained. The way those data can be used to derive the time evolution of the core field, when this is possible, or statistical information, when no other option is available, is next described. Special care is taken to explain how information derived from each type of data can be patched together into a consistent description of how the core field has been behaving in the past. Interpretations of this behavior, from the shortest (1 yr) to the longest (virtually the age of the Earth) time scales are finally reviewed, underlining the respective roles of the magnetohydodynamics at work in the core, and of the slow dynamic evolution of the planet as a whole.

5. Rainbow (MAR 36°N)的洋脊伸展，海洋核杂岩和超基性热液活动：来自多尺度磁测的约束

翻译人：李园洁 liyj3@sustech.edu.cn

摘要：在不活跃的超基性热液点 Clamstone 进行高分辨率磁测揭示出正的磁异常，这与迄今已知的其他超基性热液点的磁响应一致。这里的磁异常特征主要是热液点下的原位磁化的蛇纹岩导致，而不是网脉带磁铁矿的富集，后者由于有限的热液喷发而可以忽略不计。相反，附近的高温活跃超基性热液点 Rainbow，热液活动在超基性网脉带产生大量的磁铁矿。从更大尺度上看，我们根据海平面磁异常的分析中得出，下伏的 Rainbow Hill 作为与 Amar Minor 北段有关的一个海洋核杂岩发展起来，是由 Amar Minor 南段的向北伸展和北段的同时期后撤而拆离。这种模式解决了核杂岩（通常与冷的贫岩浆的环境有关）之上存在高温热液点的悖论：核杂岩属于冷的后撤的 Amar Minor 北段，而 Rainbow 的热流来自热的伸展的 Amar Minor 南段。这也可以解释为什么 Rainbow Hill 尽管解释为海洋核杂岩但是缺乏典型的皱褶，其是由非转换的偏移向北伸展有关的变形所拆离。

ABSTRACT：A high-resolution magnetic survey conducted over the apparently inactive ultramafic-hosted hydrothermal site Clamstone reveals a positive magnetic anomaly, in accordance with the magnetic response of other ultramafic-hosted sites known to date. Here this magnetic signature is mainly the result of inplace bulk-magnetized serpentinite underlying the site rather than any concentration of magnetite within the stockwork zone, the latter being probably negligible due to the limited fluid venting. Conversely, the nearby high-temperature active ultramafic-hosted hydrothermal site Rainbow illustrates the key contribution of hydrothermal activity in producing large amounts of magnetite in stockwork zones within ultramafics. At a larger scale, we propose from the analysis of sea-surface magnetic anomalies that the underlying Rainbow Hill has been formed as an oceanic core complex associated with the Amar Minor North segment, later dismantled by the northward propagation of the Amar Minor South segment and the coeval recession of the Amar Minor North segment. This model solves the apparent paradox of a hightemperature hydrothermal site sitting on an oceanic core complex usually associated with cold, poorly magmatic spreading environments: the core complex belongs to the cold, receding Amar Minor North segment

whereas the heat fueling site Rainbow comes from the hot, propagating Amar Minor South segment. It also explains why the Rainbow Hill, although interpreted as an oceanic core complex, lacks the typical corrugations of such core complexes – the latter have been dismantled by the deformation associated with the northward propagation of the non-transform offset.
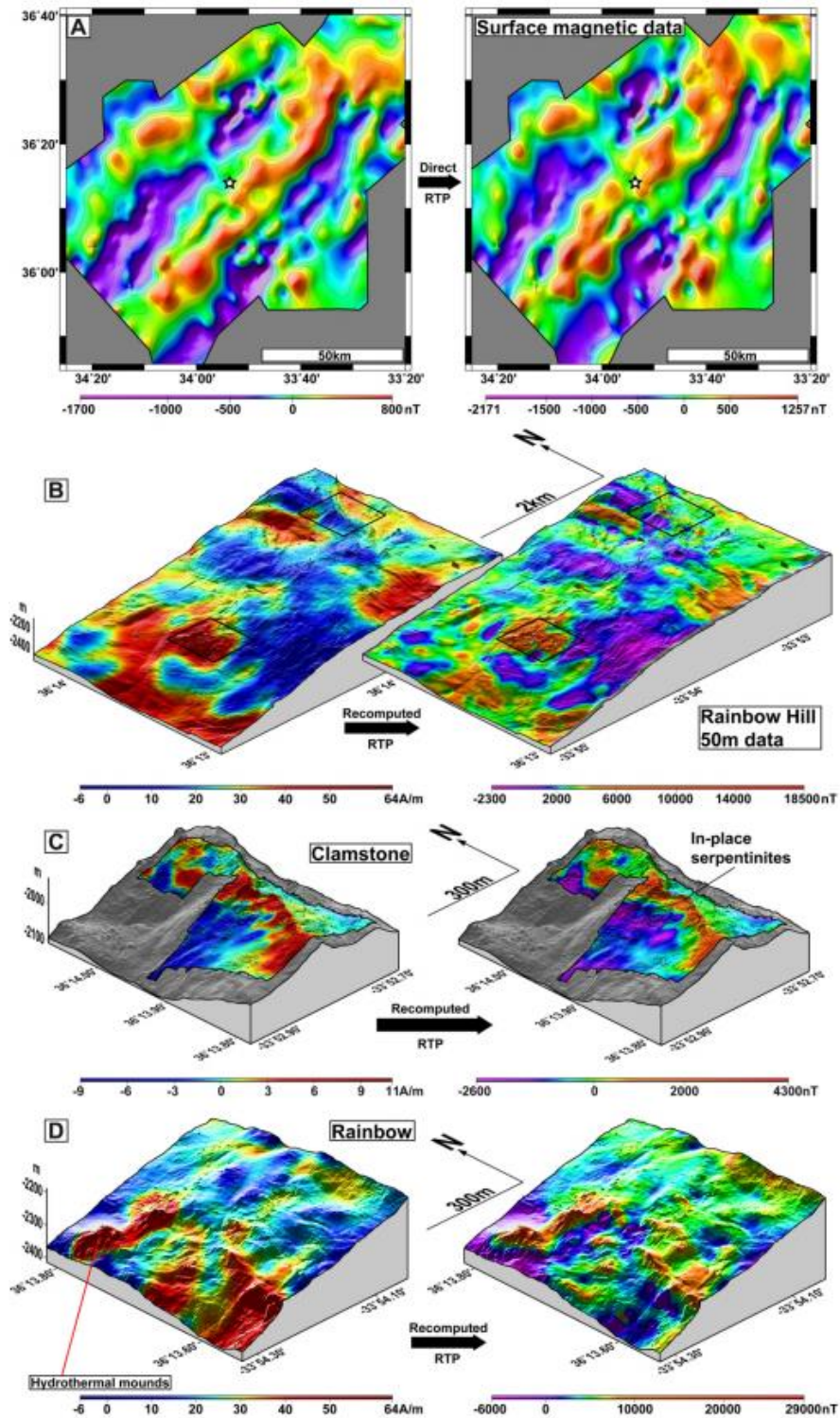

Figure 1. Magnetic anomalies in the Rainbow area at different altitudes and scales. (A) Regional sea-

surface RTP magnetic anomaly obtained by combining the available shipborne magnetic anomaly profiles. The Rainbow Hill is associated with weaker signal. Magnetic polarity reversals up to Chron 2A are seen on both ridge flanks. (B) Equivalent magnetization and RTP anomaly at 50 m altitude over the Rainbow Hill. (C) Idem as (B) for the 10 m altitude magnetic data over UMHS Clamstone. (D) Idem as (B) for the 10 m altitude magnetic data over UMHS Rainbow.
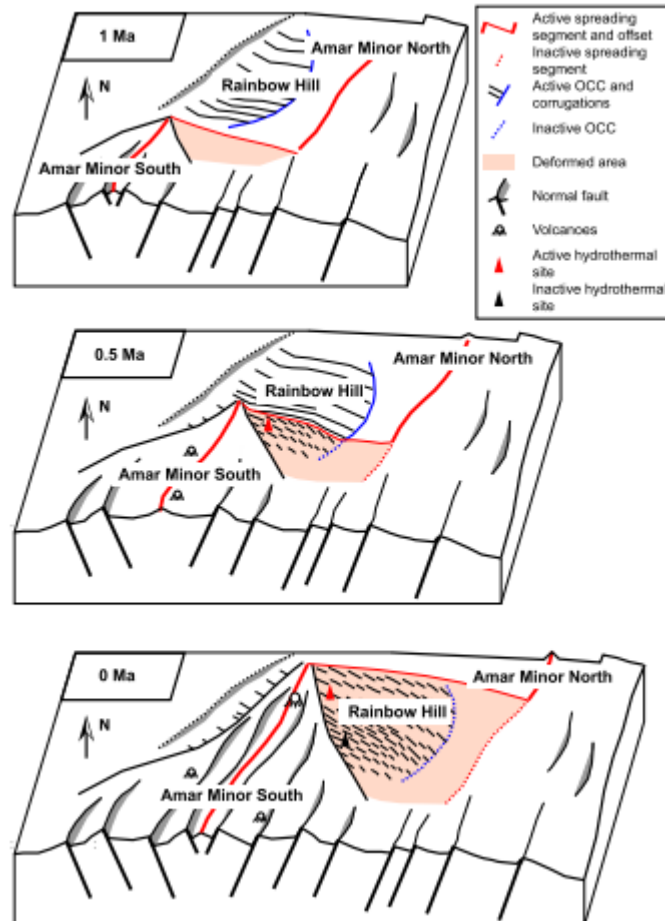

Figure 2. Proposed schematic evolution of the Rainbow area at 1 Ma, 0.5 Ma and 0 Ma. The deformed area (in red) corresponds to a sliver of crust, here the main part of an oceanic core complex (OCC), formed on the North-American plate and transferred to the African plate by the northward propagation of the Amar Minor South segment, the recession of the Amar Minor North segment, and the progressive northward shift of the non-transform offset between the two segments. The propagation isolates the body of the OCC from its breakaway, destroys the corrugations, and explains why high temperature hydrothermal sites exist on ultramafic seafloor formed at a poorly magmatic spreading center.

6. 中美洲 9000 年前稳定对流水文机制的起源

翻译人：郑威　11930589@mail.sustech.edu.cn

摘要: 很多全新世水文气候记录表明，降雨量随轨道因素引起的太阳辐射变化而变化。然而，一些热带区域的雨量演化模式与缓慢的岁差变化不同步，这表明直接的降雨驱动因素是由海表温度阈值和海洋温度梯度主导的。我们在此展示了危地马拉洞穴石笋12000年（U/Th定年）连续的降雨记录，记录表明中美洲降雨从9000年前在2000年之内从持续干旱状态转变为活跃的对流状态，并且此后依然相对活跃。我们的数据显示中美洲降雨在全新世的演变受邻近热带大洋超温度阈值驱动。因此，该区域对辐射强迫缓慢变化的敏感度很大程度上被作用于更短时间尺度的内部动力调和。

ABSTRACT： Many Holocene hydroclimate records show rainfall changes that vary with local orbital insolation. However, some tropical regions display rainfall evolution that differs from gradual precessional pacing, suggesting that direct rainfall forcing effects were predominantly driven by sea-surface temperature thresholds or inter-ocean temperature gradients. Here we present a 12,000 yr continuous U/Th-dated precipitation record from a Guatemalan speleothem showing that Central American rainfall increased within a 2000 yr period from a persistently dry state to an active convective regime at 9000 yr BP and has remained strong thereafter. Our data suggest that the Holocene evolution of Central American rainfall was driven by exceeding a temperature threshold in the nearby tropical oceans. The sensitivity of this region to slow changes in radiative forcing is thus strongly mediated by internal dynamics acting on much faster time scales.
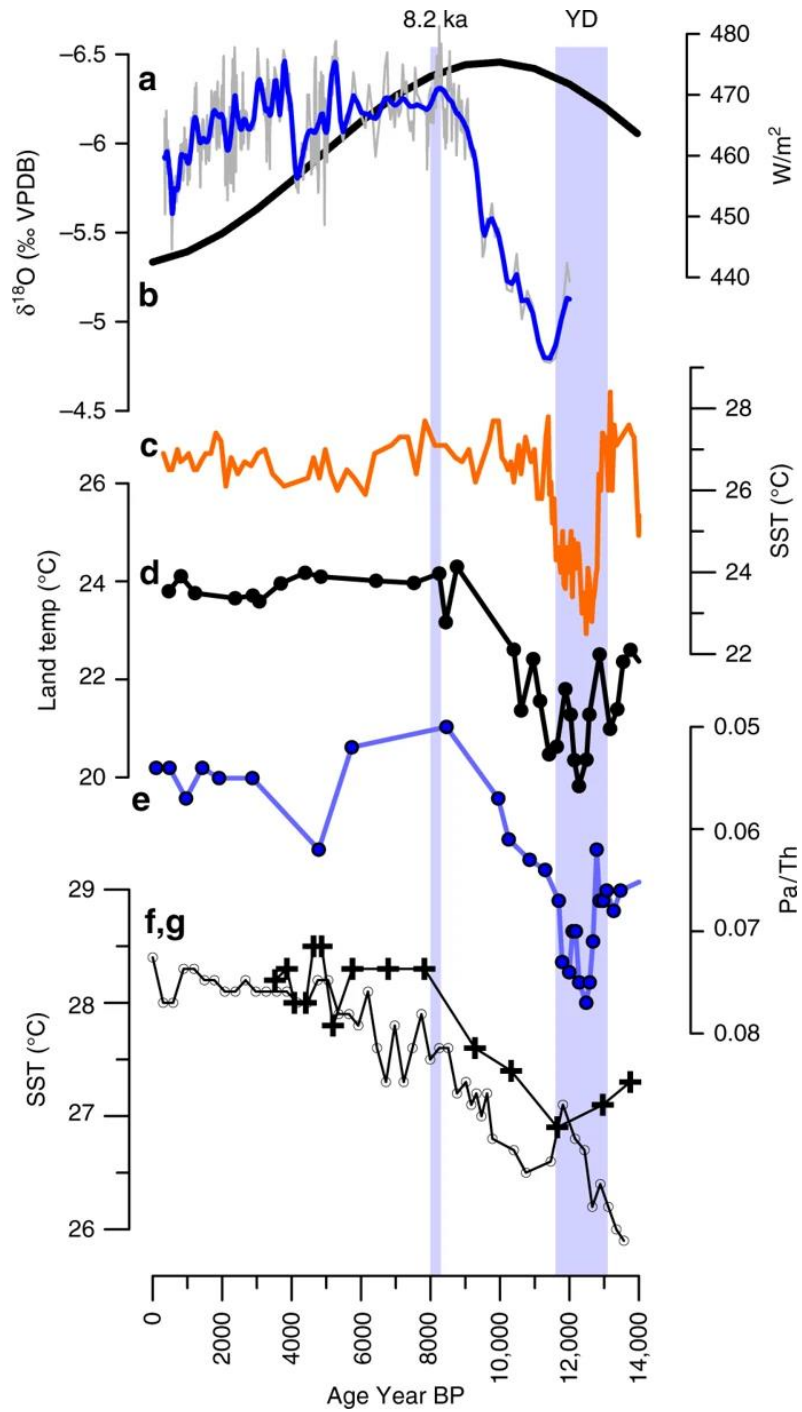
Figure 1. Comparison of **a** the Guatemala speleothem GU-RM1 precipitation proxy with **b** 15°N July 21 insolation, **c** sea-surface temperature (SST) in the Cariaco Basin from Mg/Ca proxy[57], **d** the inferred land surface temperature for the Petén region of Guatemala from pollen in Lake Petén Itza sediments[7], and **e** the Pa/Th ratio[70], a proxy for the strength of the Atlantic Meridional Overturning Circulation (AMOC), **f** the SST near Grenada[33] (gray line with circles), and **g** Caribbean SST[32] (black line with crosses).

7. 南海过去的环境和环流变化:来自深海沉积物磁性的输入

翻译人：刘伟 inewway@163.com

C. Kissel, C. Laj,, et al. Past environmental and circulation changes in the South China Sea: Input from the magnetic properties of deep-sea sediments[J]. Quaternary Science Reviews, 2020,236.

摘要：南海位于太平洋和印度洋之间的连接地带，每年主要在雨季接收大量来自汇水盆地岩石侵蚀/风化的河流沉积物。在海上，这些沉积物被不同的水团带到它们的沉积地点，它们构成了该地区过去环境研究的独特档案。深海沉积物的磁性颗粒组分虽然在体积上占少数，但只要其物源和源汇过程受到很好的约束，就能为古海洋学重建提供极为宝贵的信息。在简要描述南海的气候、沉积和海洋学背景之后，对迄今为止有关南海的磁性沉积物的文献进行了综述。我们展示了各种各样的解释/结论，认为现在对南海有关磁性沉积物的研究是相当不清晰的。在这种情况下，源区沉积物的特征是至关重要的，因此，对最近从一组河流和海洋表面沉积物样品中获得的磁性颗粒组分进行了总结，以描述当前的情况。然后，对分布于从南部到北部盆地不同水深的 7 个海相岩心用来解释古气候记录，这些海相岩心至少覆盖了最后一个气候循环。首次报道的结果表明，磁性矿物在陆地上的时间分布较为稳定，在海洋上的时间和空间分布是海平面变化和深海环流相互作用的结果。在低海平面时期，海底深海环流较弱，沉积物来源于近源河流。相反，在高海平面期间，环流增强，将更多的沉积物从台湾和吕宋岛输送到南海的西北部，也将更小比例的沉积物输送到南部盆地，与当地的来自河流的沉积物混合。通过比较两个最长的记录，我们发现这种模式在最近的 900 ka 重复出现。在 100 kyr 周期的基础上，我们还观察到一种较长周期的演变，在 500 ka 左右底流强度达到最大值，这与深海环流和碳循环的全球变化相吻合。这些基于南海众多海洋沉积岩心的磁性特征的新结果，表明磁性颗粒组分的研究对受全球气候环境变化影响的沉积路径变化、深海环流动力学具有重要意义。

ABSTRACT: The South China Sea, located at the transition between the Pacific and the Indian Ocean, receives every year, mainly during the rain season, enormous amounts of river sediments originating from the erosion/ weathering of rocks in the catchment basins. At sea, these sediments are carried by different water masses to their deposition site and they constitute a unique archive for past environmental studies in this region. The magnetic fraction of deep-sea sediments, though

forming a minority in volume, provides incredibly valuable information for paleoceanographic reconstructions, as long as its provenance and source-to-sink processes are well constrained. After a brief description of the climatic, sedimentological and oceanographic context of the South China Sea (SCS), a review of the information available so far in the literature about the magnetic properties of SCS sediments is presented. It shows a large variety of interpretations/conclusions that finally results in a rather unclear picture. Because in such a context, the characterization of the sediment at the source is critical, the magnetic properties recently obtained from a set of samples from rivers and marine surface sediments are summarized to describe the present day situation. They are then used to interpret paleorecords from a set of seven marine cores distributed from the southern to the northern basins at different water depths and all covering at least the last climatic cycle. The results reported here for the first time suggest that the magnetic mineralogy remains rather stable in time on land and that its time and spatial distribution at sea is an interplay of changes in sea level and deep-sea circulation. During low sea level periods, bottom deep-sea circulation is weak and the deposited sediment originates from the proximal rivers. On the contrary, during high sea level, the circulation is enhanced, transporting more sediment most likely from Taiwan and Luzon, to the northwestern part of the SCS and also, in smaller proportion, to the southern basin where it mixes with the local river-borne sediment. By comparing the two longest records, we observe that this pattern is repeated over the last 900 ka. Superimposed to the 100 kyr cyclicity we also observe a longer-term evolution with a maximum in the bottom current strength around 500 ka coinciding with global changes in the deep ocean circulation and carbon cycle. These new results, based on a wide spectrum of magnetic properties of numerous marine sedimentary cores from the SCS, show that the magnetic fraction yields important insights into past changes of the sedimentary pathways, in particular the dynamic of the deep-sea circulation, depending on the global climatic context.
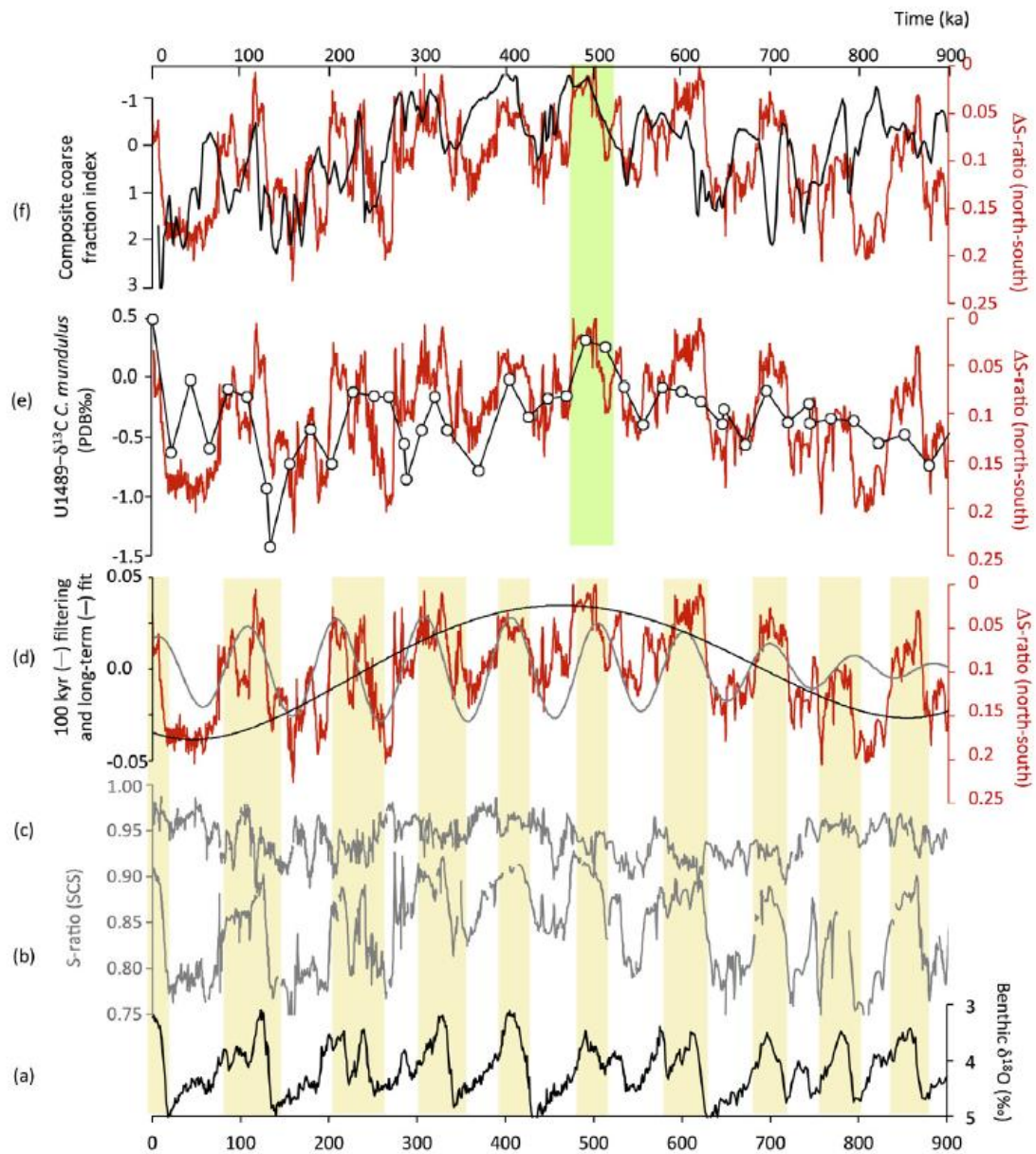
Figure 1. Variations of the S-ratio in the southern and northern basins as measured in the longest cores (ODP 1143 and 1145, respectively) covering the last 900 ka. The LR04 stack (Lisiecki and Raymo, 2005) is given as a guide for the climatic stages in (a). The two S-ratio records from southern ODP site 1143 (b) and northern ODP site 1145 (c) were used to calculate the △S-ratio between the north and the south (d). In (d), the 100 kyr filtering and long-term polynomial fit are also reported as grey and black curves, respectively. The △S-ratio is compared in (e) to the benthic d13C record from the western equatorial Pacific (Dang et al., 2020) and in (f) to the coarse fraction index produced by Bassinot et al. (1994). The light yellow vertical rectangles are for interglacial stages and the green one is for the δ13C max II coinciding with the lowest carbonate dissolution and lowest DS-ratio, all illustrating enhanced deep-sea circulation. (For interpretation of the references to color in this figure legend, the reader is referred to the Web version of this article.)

8. 石笋氧同位素记录的亚洲夏季风在冰期-间冰期的变化

翻译人：杨会会 11849590@mail.sustech.edu.cn

*Liu G, Li X, Chiang H W, et al. **On the glacial-interglacial variability of the Asian monsoon in speleothem δ¹⁸O records [J].Science Advances,** 2020, 6 : eaay8189*

摘要：尽管从中国石笋氧同位素记录中已经得到了亚洲季风清晰的变化，但记录中缺少冰期-间冰期的变化仍然令人疑惑。本文报道了三个不同地区的石笋氧同位素记录，并分析了亚洲季风降雨特征在过去 180 ka 的变化，这三个地区沿着作为亚洲季风重要支脉的印度季风轨迹分布。我们发现，靠近季风水汽来源的记录在冰期-间冰期尺度的变化很大，然后向着陆地方向冰期-间冰期变化逐渐减小。这些变化可能反映了在冰期亚洲季风水汽的逐步降雨引起的更强的氧同位素分馏过程，这可能是由冰期更大的温度梯度和受抑制的植被蒸腾作用所共同导致的。我们称这种效应为水分输送途径效应，它抵消了冰期边界条件的驱动作用。

ABSTRACT: While Asian monsoon (AM) changes have been clearly captured in Chinese speleothem oxygen isotope (δ¹⁸O) records, the lack of glacial-interglacial variability in the records remains puzzling. Here, we report speleothem δ¹⁸O records from three locations along the trajectory of the Indian summer monsoon (ISM), a major branch of the AM, and characterize AM rainfall over the past 180,000 years. We have found that the records close to the monsoon moisture source show large glacial-interglacial variability, which then decreases landward. These changes likely reflect a stronger oxygen isotope fractionation associated with progressive rainout of AM moisture during glacial periods, possibly due to a larger temperature gradient and suppressed plant transpiration. We term this effect, which counteracts the forcing of glacial boundary conditions, the moisture transport pathway effect.
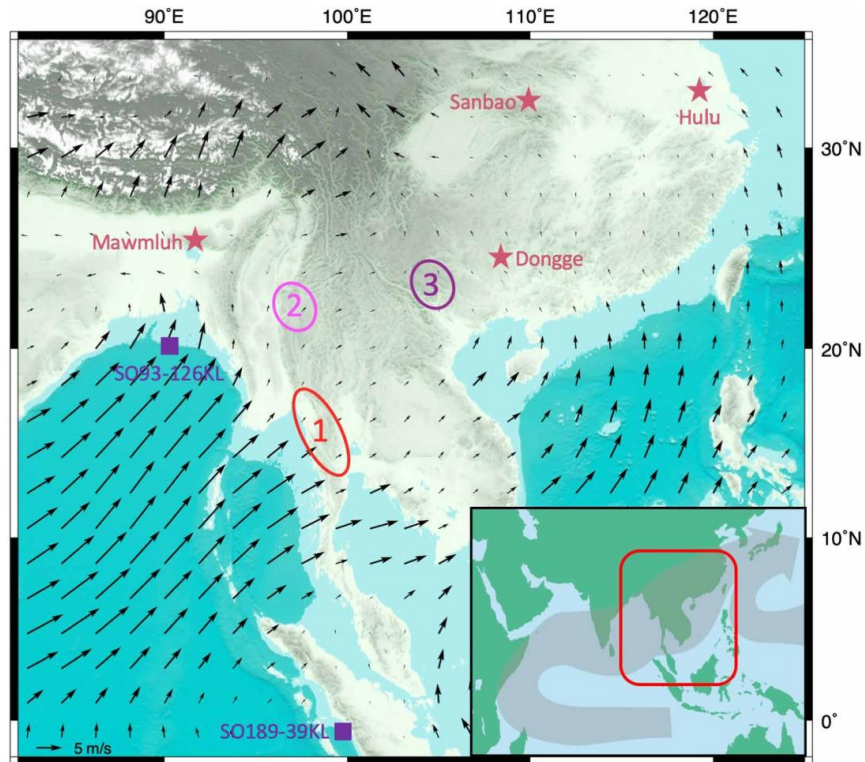
Figure 1. Sample locations. The black arrows represent the present-day averaged June-July-August (JJA) wind pattern 10 m above sea level [data from the National Centers for Environmental Prediction/National Center for Atmospheric Research Reanalysis monthly mean (1981 to 2010) (58)]. The insert shows the AM system [modified after (59)]. The circled numbers mark the three strategic cave sites along the monsoon trajectory (1, CBoB; 2, CM; and 3, SEY). The stars mark the Mawmluh (21, 26), Hulu(60), Dongge (2, 61, 62), and Sanbao (1, 2) caves; and squares mark marine sediment cores SO93-126KL (27) and SO189-39KL (39) for reference.
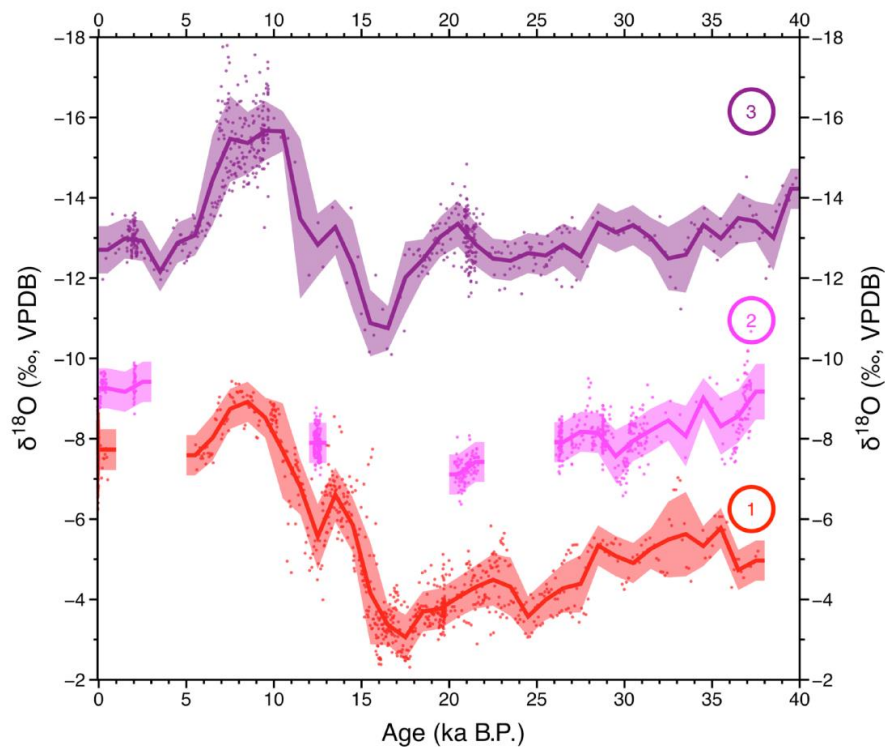
Figure 2. Spatial-temporal comparison of speleothem δ^{18}O records from mainland Southeast Asia over the past 40 ka. The records obtained from the CBoB and Mawmluh (21, 26) (site 1), CM (site 2), and SEY (site 3) caves are shown in red, pink, and purple, respectively. Note that the 18O in those records from locations other than CBoB has been corrected for temperature effect during calcite precipitation (see details in Materials and Methods). We further smoothed each record using 1000-year averages (thick lines). The shaded envelopes indicate the range of 1 uncertainty of the 18O values. The comparison shows a broad 18O-depletion trend from coastal sites to inland, associated with the progressive rainout effect on water isotopes. In addition, the isotopic gradient was larger during the LGM compared with today.
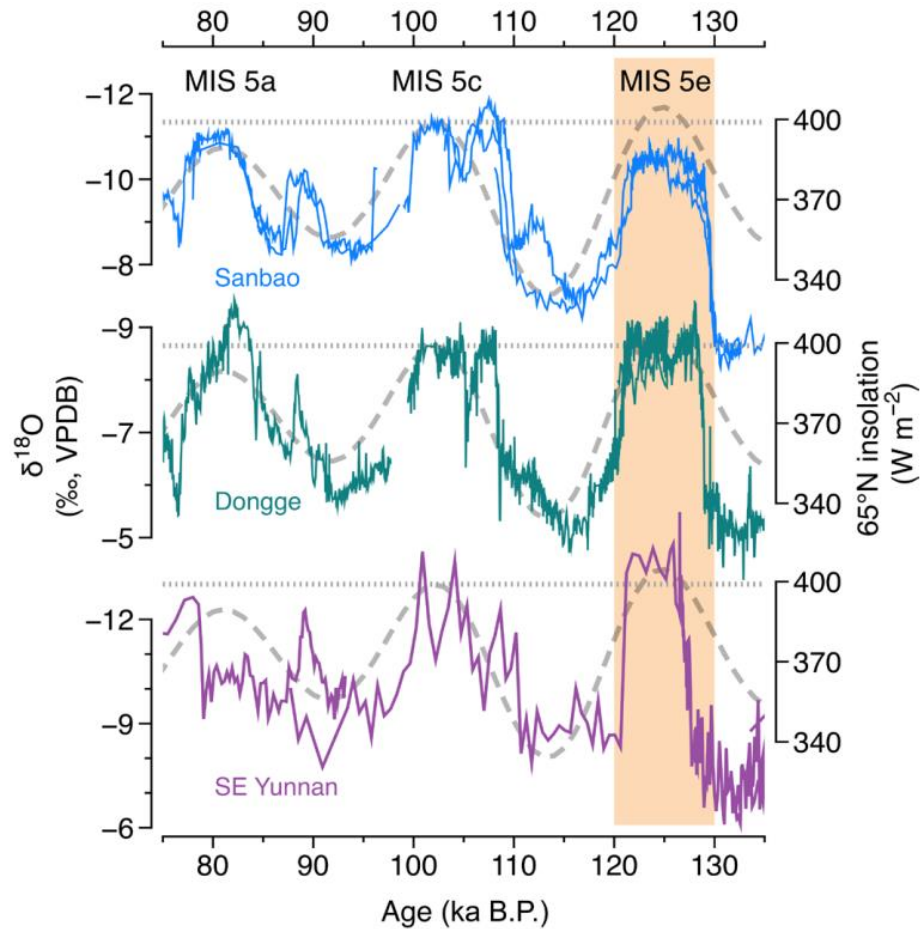

Figure 3. Spatial-temporal comparison of speleothem δ^{18}O records from the SEY, Dongge (2) and Sanbao (1) caves in southern China during MIS 5. The summer(21 July) insolation at 65°N (the gray curve) is also plotted for comparison. To facilitate the comparison, we aligned the speleothem δ^{18}O values during MIS 5c with the insolation peak. The dashed lines, drawn from the MIS 5c insolation peak, indicate the difference among the three records in their amplitudes of δ^{18}O minima during MIS 5.

9. 尼日利亚西南部 Oke-Aro 铁矿床的地面磁测调查

翻译人：曹伟 11930854@mail.sustech.edu.cn

Adebisi M A . Ground Magnetic Survey for the Investigation of Iron Ore Deposit at Oke-Aro in Iseyin East, South-Western Nigeria[J]. International Journal of Geosciences, 2018, 09(7):415-427.

摘要：在尼日利亚的西南部的 Iseyin(Lat. 7.99883˚N to Lat. 7.99933˚N, Long. 3.57900˚E to Long. 3.57990˚E)进行了一次调查是否存在铁矿藏的地面磁测。本次磁测设计了 10 条由西向东，每条 100 米，相互间隔 5 米的测线，使用质子磁力仪(G-856ax)沿测线每隔 10 米测量一次磁场强度。对所获取的磁测数据进行偏移校正，以剖面形式进行表示。我们通过计算磁异常顶部界面的深度来解释剖面，所获取的数据用来建立二维和三维磁异常图件。磁测结果将该地区划分为一些高、低磁场强度区。其中强磁场异常区表明存在高磁化率的物质，可能是铁化合物。通过对采集的数据进行定量和定性分析，为广泛分布在最大 8 nT 正异常至最小 6nT 负异常的磁异常分量提供了价值。运用 Peter 的半坡技术，获取了基底深度，实际获取最大深度为 6.25 米。根据对该地区地质背景的了解，结合磁测获取的信息，我们最终得出结论：研究区域所处的地质构造环境有利于 Oke-Aro 地区的铁矿石富集。

ABSTRACT：A ground magnetic survey was carried out to investigate the presence of iron ore at a location (Lat. 7.99883˚N to Lat. 7.99933˚N, Long. 3.57900˚E to Long. 3.57990˚E) in Iseyin, Oyo State, South-western Nigeria. Ten magnetic traverses each 100 m long at a separation of 5 m were run West-East. Magnetic intensity was taken at intervals of 10 m along each traverse line using the proton precession magnetometer (G-856 AX). The measured magnetic field data were corrected for drift and were presented as profiles. The profiles were interpreted by calculating the depth to the top of anomalies. The data obtained were used to construct magnetic anomaly maps in 2D and 3D. The magnetic survey results delineated this location into some high and low magnetic field intensity regions. The regions of high magnetic field anomaly indicated the presence of materials with high susceptibility which was suspected to be iron compounds. The quantitative and qualitative analyses on interpretations of field data collected were given, while these results provided values for the total component measurements of ground magnetic anomaly that widely ranged between a maximum

positive peak result of 8 nT and to a minimum negative peak result of −6 nT. Using Peter's half slope technique, depth to the basement was assessed, which actually provided a maximum depth to basement of 6.25 m. From the knowledge of the geology of the area and also, the magnetic survey employed information, therefore, we can finally conclude that, the study area is under laid by geologic structures which favour the accumulation of iron-ore minerals deposit at Oke-Aro area in Iseyin.
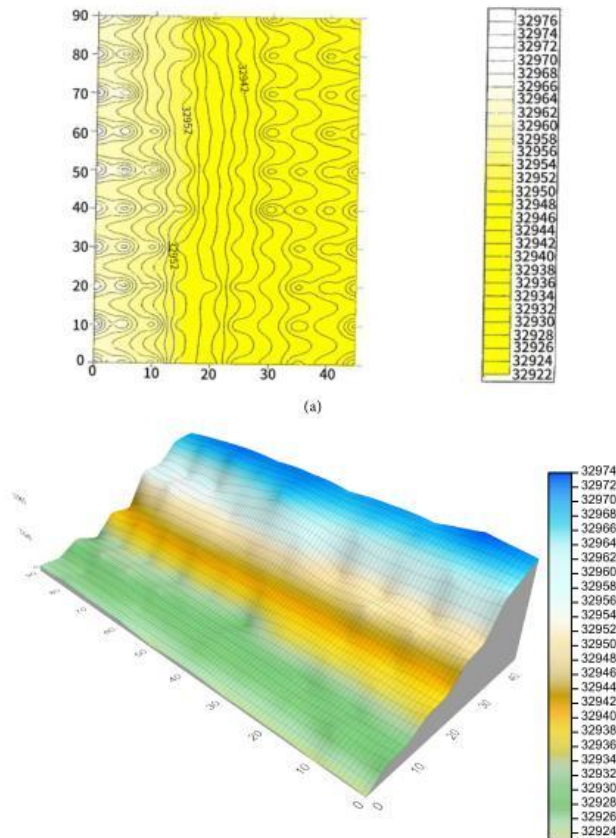

Figure 1. Revealed the magnetic-field in (a) 2-Dimensional, (b) 3-Dimensional contour map plotted for the whole survey area.

10. 海洋中金属元素在生物和非生物作用下的滞留、再循环和矿化过程

翻译人：王敦繁

*Boyd P W, Ellwood M J, Tagliabue A, et al. **Biotic and abiotic retention, recycling and remineralization of metals in the ocean[J]. Nature Geoscience,** 2017, 10(3):167-173.*

摘要：海洋中的生物地球化学循环过程以及海洋中的生物生态结构都与微量金属元素密切相关，目前人们对海洋中微量金属元素生物地球化学过程的研究主要聚焦在其外源输入模式上，比如粉尘输入，热液活动以及沉积作用等。然而，海洋中的金属元素也存在其内部的转化过程，比如在生物或非生物作用下的滞留，再循环以及矿化过程。人们现在对金属元素生物地球化学作用的研究也越来越关注其在内部的转化过程。首先，在生物作用下金属元素在海水表层的滞留时间可达数天或数周甚至数月，并由浮游生物所能够利用的元素种类和其最终归宿所决定，比如从病毒溶解到赋存时间再到被捕食并最终输送到海底。相比单独的外源输入，海洋表层金属元素快速的再循环作用更能通过保持高水平的生物可利用性促进其季节性的生产力水平。随着含金属元素的有机颗粒从海洋表面输送下来，不同的金属元素在不同深度表现出不同的再矿化模式。这些模式是由一系列广泛的物理化学和微生物过程调节的，比如颗粒吸附金属的能力，以及沉降颗粒的矿物和有机特征。研究表明金属元素的内部转化过程在控制金属的生物利用度、浮游植物分布以及深部金属元素再补给方面起着重要作用。

ABSTRACT: Trace metals shape both the biogeochemical functioning and biological structure of oceanic provinces. Trace metal biogeochemistry has primarily focused on modes of external supply of metals from aeolian, hydrothermal, sedimentary and other sources. However, metals also undergo internal transformations such as abiotic and biotic retention, recycling and remineralization. The role of these internal transformations in metal biogeochemical cycling is now coming into focus. First, the retention of metals by biota in the surface ocean for days, weeks or months depends on taxon-specific metal requirements of phytoplankton, and on their ultimate fate: that is, viral lysis, senescence, grazing and/or export to depth. Rapid recycling of metals in the surface ocean can extend seasonal productivity by maintaining higher levels of metal bioavailability compared to the influence of external metal input alone. As metal-containing organic particles are exported from the surface ocean, different metals exhibit distinct patterns of remineralization with depth. These

patterns are mediated by a wide range of physicochemical and microbial processes such as the ability of particles to sorb metals, and are influenced by the mineral and organic characteristics of sinking particles. We conclude that internal metal transformations play an essential role in controlling metal bioavailability, phytoplankton distributions and the subsurface resupply of metals.
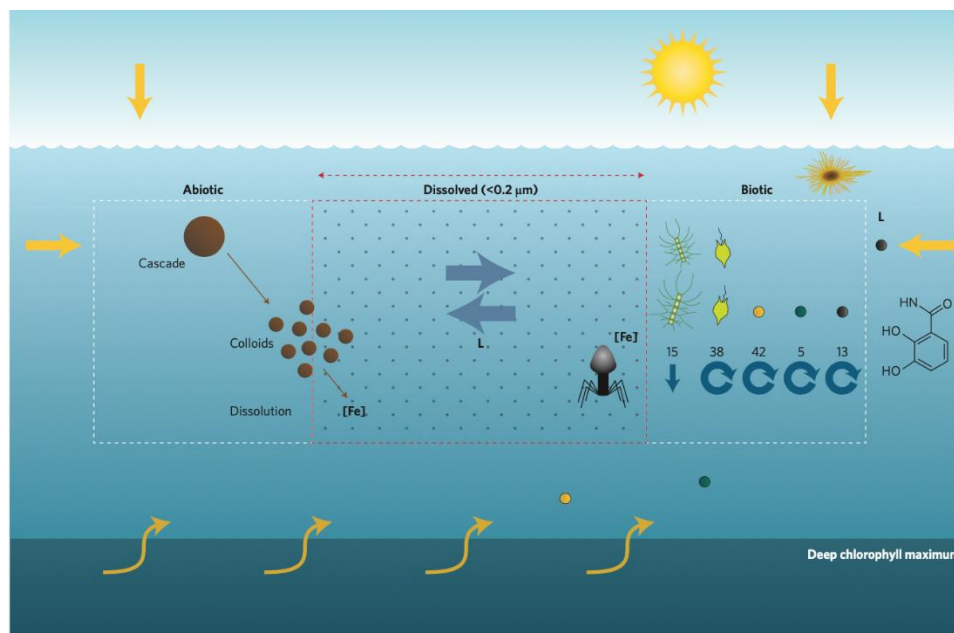

Figure 1: Schematic of modes of 'new' iron supply (orange arrows) and iron retention mechanisms within the surface mixed layer. Abiotic retention (left box) includes rapid transfer of aerosol iron to soluble pools (that is, Cascade7) and photochemically mediated colloid dissolution34. Biotic retention (right box) is driven by acquisition (for example, aerosol capture by diazotrophs36) and interactions between iron supply, differing iron quotas (pmol l–1) within natural communities (left-to-right: diatom39, autotrophic flagellate39, picoprokaryote39, picoeukaryote39, heterotrophic bacterium39) and their fate (export (downward blue arrow) or grazing/lysis (circular blue arrows)). Microbial ligand (L) release retains metals in solution (denoted by the partial chemical structure of the enterobactin siderophore) and is stimulated by new metal supply25,26. The virus represents putative iron recycling through progeny phages33. Horizontal blue arrows denote exchange between the dissolved and other pools mediated by ligands.